

# A Shearlet Approach to Edge Analysis and Detection

Sheng Yi, Demetrio Labate, Glenn R. Easley, and Hamid Krim

**Abstract**—It is well known that the wavelet transform provides a very effective framework for analysis of multiscale edges. In this paper, we propose a novel approach based on the shearlet transform: a multiscale directional transform with a greater ability to localize distributed discontinuities such as edges. Indeed, unlike traditional wavelets, shearlets are theoretically optimal in representing images with edges and, in particular, have the ability to fully capture directional and other geometrical features. Numerical examples demonstrate that the shearlet approach is highly effective at detecting both the location and orientation of edges, and outperforms methods based on wavelets as well as other standard methods. Furthermore, the shearlet approach is useful to design simple and effective algorithms for the detection of corners and junctions.

**Index Terms**—Curvelets, edge detection, feature extraction, shearlets, singularities, wavelets.

## I. INTRODUCTION

Edges are prominent features in images and their analysis and detection are an essential goal in computer vision and image processing. Indeed, identifying and localizing edges are a low level task in a variety of applications such as 3D reconstruction, shape recognition, image compression, enhancement and restoration.

In this paper, we apply a novel directional multiscale mathematical framework which is especially adapted to identification and analysis of distributed discontinuities such as edges occurring in natural images. Multiscale methods based on wavelets, have been successfully applied to the analysis and detection of edges [1], [2], [3], [4], [5]. Despite their success, wavelets are however known to have a limited capability in dealing with directional information. By contrast, the shearlet approach, which we propose here, is particularly designed to deal with directional and anisotropic features typically present in natural images, and has the ability to accurately and efficiently capture the geometric information of edges. As a result, the shearlet framework provides highly competitive algorithms, for detecting both the location and orientation of edges, and for ex-

tracting and classifying basic edge features such as corners and junctions.

Our shearlet approach has similarities with a number of other methods in applied mathematics and engineering to overcome the limitations of traditional wavelets. These methods include *contourlets* [6], [7] *complex wavelets* [8], *ridgelets* [9] and *curvelets* [10]. In contrast to all these methods, the shearlet framework provides a unique combination of mathematical rigidity and computational efficiency when addressing edges, optimal efficiency in dealing with edges, and computational efficiency. In addition, its continuous formulation is particularly well-suited for designing an implementation, presented in this work, for the purpose of edge analysis and detection.

### A. Edge detection using wavelets.

In the classic Canny edge detection algorithm [11], an image  $u$  is smoothed by a convolution with a Gaussian filter:

$$u_a = u * G_a, \quad (\text{I.1})$$

where  $G_a(x) = a^{-1} G(a^{-1}x)$ , for  $a > 0$ , and  $G(x)$  is the Gaussian function. Edges are then recognized as the local maxima of the magnitude of the gradient of  $u_a$ . The adjustable scaling factor  $a$  determines the amount of smoothing: as  $a$  increases, the detector's sensitivity to noise decreases; however, as  $a$  increases, the localization error in the detection of edges also increases. As a result, the performance of the algorithm heavily depends on the scaling factor  $a$  [12], [13].

It was observed by Mallat et al. [1], [2] that, at a single scale, the Canny edge detector is equivalent to the detection of the local maxima of the wavelet transform of  $u$ , for some particular choices of the analyzing wavelet. In fact, the function  $\psi = \nabla G$  is a wavelet known as the *first derivative Gaussian wavelet*. Thus, each image  $u \in L^2(\mathbb{R}^2)$  satisfies:

$$u(x) = \int W_\psi u(a, y) \psi_a(x - y) dy,$$

where  $\psi_a(x) = a^{-1} \psi(a^{-1}x)$ , and  $W_\psi u(a, x)$  is the *wavelet transform* of  $u$ , defined by

$$W_\psi u(a, x) = \int u(y) \psi_a(x - y) dy = u * \psi_a(x).$$

D. Labate, S. Yi and H. Krim are with North Carolina State University, Raleigh, NC 27695, USA (dlabate@math.ncsu.edu; syi@ncsu.edu; ahk@eos.ncsu.edu)

S. Yi and H. Krim were in part funded by AFOSR, AF9550-07-1-0104. DL acknowledges partial support from NSF DMS 0604561 and DMS (Career) 0746778

G. R. Easley is with System Planning Corporation 1000 Wilson Boulevard, Arlington, VA 22209, USA (geasley@sysplan.com)

The significance of this representation is that the wavelet transform provides a space-scale decomposition of the image  $u$ , where  $u \in L^2(\mathbb{R}^2)$  is mapped into the coefficients  $W_\psi u(a, y)$  which depend on the location  $y \in \mathbb{R}^2$  and the scaling variable  $a > 0$ . Another useful observation is that the wavelet transform of  $u$  is proportional to the gradient of the smoothed image  $u_a$ :

$$\nabla u_a(x) = u * \nabla G_a(x) = u * \psi_a(x) = W_\psi u(a, x). \quad (1.2)$$

This shows that the maxima of the magnitude of the gradient of the smoothed image  $u_a$  correspond exactly to the maxima of the magnitude of the wavelet transform  $W_\psi u(a, x)$ ; this provides a natural mathematical framework for the multiscale analysis of edges [1], [2]. In particular, utilizing multiscale wavelet representation avoids the problem of finding the appropriate scale  $a$  which produces an improved detection of the classic Canny algorithm. Furthermore, there are very efficient numerical implementations of the wavelet transform [14].

The difficulty of edge detection is particularly prominent in the presence of noise, and when several edges are close together or cross each other, e.g., 2-dimensional projections of 3-dimensional objects [15]. In such cases, the following limitations of the wavelet approach (and other traditional edge detectors) become evident:

- *Difficulty in distinguishing close edges.* The isotropic Gaussian filtering causes edges running close together to be blurred into a single curve.
- *Poor angular accuracy.* In the presence of sharp changes in curvature or crossing curves, the isotropic Gaussian filtering leads to an inaccurate detection of edge orientation. This affects the detection of corners and junctions.

To address these difficulties one has to account for the anisotropic nature of edge lines and curves. For example, in [16], [17], [18] it is proposed to replace the scalable collection of isotropic Gaussian filters  $G_a(x_1, x_2)$ ,  $a > 0$  in (I.1) with a family of steerable and scalable anisotropic Gaussian filters

$$G_{a_1, a_2, \theta}(x_1, x_2) = a_1^{-1/2} a_2^{-1/2} R_\theta G(a_1^{-1} x_1, a_2^{-1} x_2),$$

where  $a_1, a_2 > 0$  and  $R_\theta$  is the rotation matrix by  $\theta$ . Unfortunately, the design and implementation of such filters is computationally demanding. In addition, the justification for this approach is essentially intuitive, and there is no proper theoretical model to indicate how to “optimize” such family of filters to best capture edges.

### B. The Shearlet Approach.

The approach proposed in this paper is based on a new multiscale transform called the *shearlet transform*.

This transform, introduced by the authors and their collaborators in [19], [20], is a genuinely multidimensional version of the traditional wavelet transform, and is especially designed to address anisotropic and directional information at various scales. Indeed, the traditional wavelet approach, which is based on isotropic dilations, has a very limited capability to account for the geometry of multidimensional functions. In contrast, the analyzing functions associated to the shearlet transform are highly anisotropic, and, unlike traditional wavelets, are defined at various scales, locations and orientations. As a consequence, this transform provides an optimally efficient representation of images with edges [21].

The shearlet transform has similarities to the curvelet transform, first introduced by Candès and Donoho [10], [22]. Shearlets and curvelets, in fact, are the only two systems which were mathematically known to provide optimally sparse representations of images with edges. The spatial-frequency tilings of the two representations are completely different, yet the implementations of the curvelet transform corresponds to essentially the same tiling as that of the shearlet transform. In spite of this similarity, it is not clear how the curvelet transform implementations could be modified to do the applications described in this paper. Yet an application of low-level vision using curvelets has been suggested in [23].

Both systems are related to contourlets [6], [7] and steerable filters [24], [25]. Contourlets, however, provide a purely discrete approach which presents difficulties in rigorously addressing the edge detection problem. We refer to [19] for more details about the comparison of shearlets and other orientable multiscale transforms.

In this paper, we combine the shearlet framework with several well established ideas from the image processing literature to obtain improved and computationally efficient algorithms for edge analysis and detection. Our approach may be viewed as a truly multidimensional refinement of the approach of Mallat et al., where the isotropic wavelet transform  $W_\psi u(a, x)$  is replaced by an anisotropic directional multiscale transform. Specifically, for an image  $u$ , the shearlet transform is a mapping

$$u \rightarrow \mathcal{SH}_\psi u(a, s, x),$$

depending on the scale  $a > 0$ , the orientation  $s$  and the location  $x$ . This provides a *directional* scale-space decomposition of  $u$  and, as shown below, a theoretical justifiable framework for the identification and analysis of the edges of  $u$ . The shearlet transform can be expressed as

$$\mathcal{SH}_\psi u(a, s, x) = \int u(y) \psi_{as}(x - y) dy = u * \psi_{as}(x).$$

where the analyzing elements  $\psi_{as}$  are well localized

waveforms at various scales and orientations. As a result, the shearlet transform acts as a *multiscale directional* difference operator and provides a number of very useful features:

- *Improved accuracy in the detection of edge orientation.* Using anisotropic dilations and multiple orientations, the shearlet transform precisely captures the geometry of edges.
- *Well organized multiscale structure.* It is a multiscale transform, based on the same affine mathematical structure of traditional wavelets.
- *Computational efficiency.* The discretization of the shearlet transform provides a stable and computationally efficient decomposition and reconstruction algorithm for images.

The paper is organized as follows. Section II recalls the basic definitions and properties of the shearlet transform. Section III presents a new numerical implementation of the shearlet transform consistent with the theoretical requirements for the analysis of edges. Section IV describes applications of the shearlet approach to the estimation of edge orientation, feature classification and edge detection.

## II. SHEARLET TRANSFORM

Let  $G$  be a subgroup of the group of  $2 \times 2$  invertible matrices. The *affine systems* generated by  $\psi \in L^2(\mathbb{R}^2)$  are the collections of functions:

$$\psi_{M,t}(x) = |\det M|^{-\frac{1}{2}} \psi(M^{-1}(x-t)), \quad t \in \mathbb{R}^2, M \in G. \quad (\text{II.3})$$

If any  $u \in L^2(\mathbb{R}^2)$  can be recovered via the reproducing formula

$$u = \int_{\mathbb{R}^n} \int_G \langle u, \psi_{M,t} \rangle \psi_{M,t} d\lambda(M) dt,$$

where  $\lambda$  is a measure on  $G$ , then  $\psi$  is a *continuous wavelet* [14]. In this case, the *continuous wavelet transform* is the mapping

$$u \rightarrow W_\psi u(M, t) = \langle u, \psi_{M,t} \rangle, \quad (\text{II.4})$$

for  $(M, t) \in G \times \mathbb{R}^2$ . There are a variety of examples of wavelet transforms. The simplest case is when the matrices  $M$  have the form  $aI$ , where  $a > 0$  and  $I$  is the identity matrix. In this situation, one obtains the *isotropic* continuous wavelet transform:

$$W_\psi u(a, t) = a^{-1} \int_{\mathbb{R}} u(x) \overline{\psi(a^{-1}(x-t))} dx,$$

where the dilation factor is the same for all coordinate directions. This is the “standard” wavelet transform used in most wavelet applications (including the wavelet-based edge detection by Mallat et al. described in Section I).

It is known that the continuous wavelet transform has the ability to identify the singularities of a signal. In fact, if a function  $u$  is smooth apart from a discontinuity at a point  $x_0$ , then the continuous wavelet transform  $W_\psi u(a, t)$  decays rapidly as  $a \rightarrow 0$ , unless  $t$  is near  $x_0$  [26]. This property is useful to identify the set of points where  $u$  is not regular, and explains the ability of the continuous wavelet transform to detect edges. However, the isotropic continuous wavelet transform is unable to provide additional information about the *geometry* of the set of singularities of  $u$ . In many situations, including edge detection, it is useful to not only identify the location of edges, but also to capture their geometrical properties, such as the edge orientation. As shown by the authors and their collaborators in [27], [28], this can be achieved by employing a non-isotropic version of the continuous wavelet transform (II.4) called the *continuous shearlet transform*. This is defined as the mapping

$$\mathcal{SH}_\psi u(a, s, t) = \langle u, \psi_{ast} \rangle, \quad (\text{II.5})$$

where  $\psi_{ast}(x) = |\det M_{as}|^{-\frac{1}{2}} \psi(M_{as}^{-1}(x-t))$ , and  $M_{as} = \begin{pmatrix} a & -\sqrt{as} \\ 0 & \sqrt{a} \end{pmatrix}$  for  $a > 0, s \in \mathbb{R}, t \in \mathbb{R}^2$ . Observe that  $M_{as} = B_s A_a$ , where  $A_a = \begin{pmatrix} a & 0 \\ 0 & \sqrt{a} \end{pmatrix}$  and  $B_s = \begin{pmatrix} 1 & -s \\ 0 & 1 \end{pmatrix}$ . Hence to each matrix  $M_{as}$  are associated two distinct actions: an *anisotropic* dilation produced by the matrix  $A_a$  and a *shearing* produced by the non-expansive matrix  $B_s$ .

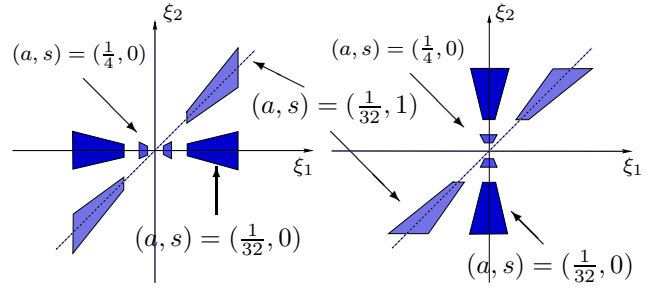


Fig. 1. Frequency support of the horizontal shearlets (left) and vertical shearlets (right) for different values of  $a$  and  $s$ .

The generating function  $\psi$  is a well localized function satisfying appropriate admissibility conditions [27], [28], so that each  $u \in L^2(\mathbb{R}^2)$  has the representation

$$u = \int_{\mathbb{R}^2} \int_{-\infty}^{\infty} \int_0^{\infty} \langle u, \psi_{ast} \rangle \psi_{ast} \frac{da}{a^3} ds dt.$$

In particular, for  $\xi = (\xi_1, \xi_2) \in \mathbb{R}^2$ ,  $\xi_1 \neq 0$ , we set  $\hat{\psi}(\xi) = \hat{\psi}_1(\xi_1) \hat{\psi}_2(\frac{\xi_2}{\xi_1})$ , where  $\hat{\psi}_1, \hat{\psi}_2$  are smooth func-

tions with  $\text{supp } \hat{\psi}_1 \subset [-2, -\frac{1}{2}] \cup [\frac{1}{2}, 2]$  and  $\text{supp } \hat{\psi}_2 \subset [-1, 1]$ . In addition, to obtain the edge detection results presented in the next section,  $\hat{\psi}_1$  (respectively,  $\hat{\psi}_2$ ) is assumed to be odd (respectively, even). In the frequency domain:

$$\hat{\psi}_{ast}(\xi_1, \xi_2) = a^{\frac{3}{4}} e^{-2\pi i \xi t} \hat{\psi}_1(a \xi_1) \hat{\psi}_2(a^{-\frac{1}{2}}(\frac{\xi_2}{\xi_1} - s)),$$

and, thus, each function  $\hat{\psi}_{ast}$  is supported in the set

$$\{(\xi_1, \xi_2) : \xi_1 \in [-\frac{2}{a}, -\frac{1}{2a}] \cup [\frac{1}{2a}, \frac{2}{a}], |\frac{\xi_2}{\xi_1} - s| \leq \sqrt{a}\}.$$

Thus each shearlet  $\psi_{ast}$  has frequency support on a pair of trapezoids, at various scales, symmetric with respect to the origin and oriented along a line of slope  $s$ . As a result, the shearlets form a collection of well-localized waveforms at various scales  $a$ , orientations  $s$  and locations  $t$ .

Notice that the shearing variable  $s$  corresponds to the slope of the line of orientation of the shearlet  $\hat{\psi}_{ast}$ , rather than its angle with respect to the  $\xi_1$  axis<sup>1</sup>. It follows that the shearlets provide a nonuniform angular covering of the frequency plane when the variable  $s$  is discretized, and this can be a disadvantage for the numerical implementation of the shearlet transform. To avoid this problem, the continuous shearlet transform is modified as follows. In the definition of  $\mathcal{SH}_\psi$ , given by (II.5), the values of  $s$  will be restricted to the interval  $[-1, 1]$ . Under this restriction, in the frequency plane, the collection of shearlets  $\psi_{ast}$  will only cover the horizontal cone  $\{(\xi_1, \xi_2) : |\frac{\xi_2}{\xi_1}| \leq 1\}$ . To compensate for this, we add a similarly defined second shearlet transform, whose analyzing elements are the “vertical” shearlets  $\psi_{ast}^{(1)}$ . In the frequency plane they are obtained from the corresponding “horizontal” shearlets  $\psi_{ast}$  through a rotation by  $\pi/2$ . The frequency supports of some representative horizontal and vertical shearlets are illustrated in Figure 1. By combining the two shearlet transforms, any  $u \in L^2(\mathbb{R}^2)$  can be reproduced with respect to the combination of vertical and horizontal shearlets. We refer to [27], [28] for additional details about this construction. In the following, when it will be needed to distinguish the two transforms we will use the notation  $\mathcal{SH}_\psi^{(0)}$  (respectively,  $\mathcal{SH}_\psi^{(1)}$ ) for the continuous shearlet transform associated to the horizontal cone (respectively, the vertical cone).

#### A. Edge resolution using the shearlet transform

The continuous shearlet transform is able to precisely capture the geometry of edges. Indeed, the asymp-

<sup>1</sup> The curvelets are indexed by scale, angle and location, where the angle is the angle of orientation in polar coordinates. The drawback of this representation, however, is that curvelets do not form an affine system, as in (II.3), and are not obtained from a single generating function.

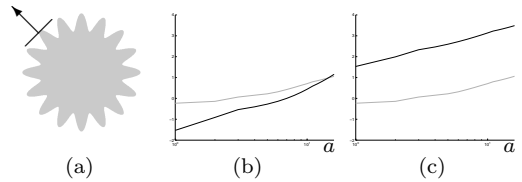


Fig. 2. Analysis of the edge response. The magnitudes of the shearlet (respectively, wavelet) transform of an edge point on the star-shaped figure (a) are plotted on a logarithmic scale as a black (respectively, gray) line. Figure (b) shows the response of the shearlet transform when its orientation variable is tangent to the edge. Figure (c) shows the response when the orientation variable is normal to the edge.

otic decay rate of the continuous shearlet transform  $\mathcal{SH}_\psi u(a, s, t)$ , for  $a \rightarrow 0$  (fine scales), can be used to obtain *both location and orientation* of edges in an image  $u$ . This is a significant refinement with respect to traditional wavelets, which only detect the location. We now present a brief summary of the most relevant results which are useful for our analysis. We refer to [27], [28] for more details.

To model an image, let  $\Omega = [0, 1]^2$  and consider the partition  $\Omega = \bigcup_{n=1}^L \Omega_n \cup \Gamma$ , where:

1. each “object”  $\Omega_n$ , for  $n = 1, \dots, L$ , is a connected open set (domain);
2. the set of edges of  $\Omega$  be given by  $\Gamma = \bigcup_{n=1}^L \partial\Omega_n$ , where each boundary  $\partial\Omega_n$  is a smooth curve of finite length.

Consider the space of images  $I(\Omega)$  defined as the collection of functions which have the form

$$u(x) = \sum_{n=1}^L u_n(x) \chi_{\Omega_n}(x) \text{ for } x \in \Omega \setminus \Gamma$$

where, for each  $n = 1, \dots, L$ ,  $u_n \in C_0^1(\Omega)$  has bounded partial derivatives, and the sets  $\Omega_n$  are pairwise disjoint in measure. For  $u \in I(\Omega)$ , we have the following results.

*Theorem II.1:* If  $t \notin \Gamma$ , then

$$\lim_{a \rightarrow 0} a^{-\frac{3}{4}} \mathcal{SH}_\psi u(a, s, t) = 0. \quad (\text{II.6})$$

If  $t \in \Gamma$  and, in a neighborhood of  $t = (t_1, t_2)$ , the boundary curve is parametrized as  $(E(t_2), t_2)$ , and  $s \neq -E'(t_2)$ , then also (II.6) holds. Otherwise, if  $s = -E'(t_2)$ , there is a constant  $C > 0$  such that

$$\lim_{a \rightarrow 0} a^{-\frac{3}{4}} \mathcal{SH}_\psi u(a, s, t) = C |[u]_t|,$$

where  $[u]_t$  is the jump of  $u$  at  $t$ , occurring in the normal direction to the edge.

This shows that asymptotic decay of the continuous shearlet transform of  $u$  is the slowest for  $t$  on the boundary of  $\Omega$ , and  $s$  corresponding to the normal orientation

to  $\Omega$  at  $t$  (see Figure 2). Other useful results from [27], [28] are the following:

- If  $u \in I(\Omega)$  and  $t$  is away from the edges, then  $\mathcal{SH}_\psi u(a, s, t)$  decays rapidly as  $a \rightarrow 0$ , and the decay rate depends on the local regularity of  $u$ . In particular, if  $u$  is Lipschitz- $\alpha$  near  $t_0 \in \mathbb{R}^2$ , then the following estimates hold: for  $\alpha \geq 0$ ,

$$|\mathcal{SH}_\psi u(a, s, t_0)| \leq C a^{\frac{1}{2}(\alpha + \frac{3}{2})}, \quad \text{as } a \rightarrow 0;$$

while for  $\alpha < 0$ ,

$$|\mathcal{SH}_\psi u(a, s, t_0)| \leq C a^{(\alpha + \frac{3}{4})}, \quad \text{as } a \rightarrow 0.$$

We refer to [14] for the definition of Lipschitz regularity. Classification of points by their Lipschitz regularity is important as it can be used to distinguish true edge points from points corresponding to noise [1], [2].

- If  $u$  contains a corner point, then locally, as  $a \rightarrow 0$ ,  $\mathcal{SH}_\psi u(a, s, t)$  decays as  $a^{3/4}$  when  $s$  is the direction normal to the edges. It decays as  $a^{5/4}$  otherwise.
- Spike-type singularities produce a different behavior for the decay of the shearlet transform. Consider, for example, the Dirac delta centered at  $t_0$ . Then

$$|\mathcal{SH}_\psi \delta_{t_0}(a, s, t_0)| \asymp a^{-3/4}, \quad \text{as } a \rightarrow 0,$$

so that the transform actually grows at fine scales. The decay is rapid for  $t \neq t_0$ .

These observations show that the geometric information about the edges of  $u$  can be completely resolved by looking at the values of its continuous shearlet transform  $\mathcal{SH}_\psi u(a, s, t)$  at fine scales. Additionally, similar to the wavelet case, the behavior of the decay rate across scales provides useful information about the regularity of  $u$ . In the following sections, we will take advantage of these properties to design improved numerical algorithms for the analysis and detection of edges.

### III. A DISCRETE SHEARLET TRANSFORM FOR EDGE DETECTION

A numerically efficient implementation of the shearlet transform was previously introduced in [19]. It was based on the use of a Laplacian pyramid combined with appropriate shearing filters. That particular implementation, however, was specially designed for image denoising. Since its direct application to edge detection suffers from large sidelobes around prominent edges (which is the same problem with the curvelet implementations), a different implementation will be presented here. This new implementation is based on separately calculating the vertical and horizontal shearlets and is

amenable to a continuous (non-dyadic) scaling. For its development, consistent with the theoretical analysis in [28], special properties on the shearlet generating function  $\psi$  (see Sec. II) are utilized.

We start by reformulating the operations associated with the shearlet transform in a way which is suitable to its numerical implementation. For  $\xi = (\xi_1, \xi_2) \in \widehat{\mathbb{R}}^2$ ,  $a < 1$ , and  $|s| \leq 1$ , let

$$\widehat{w}_{a,s}^{(0)}(\xi) = a^{-\frac{1}{4}} \overline{\widehat{\psi}_2(a^{-\frac{1}{2}}(\frac{\xi_2}{\xi_1} - s))} \chi_{\mathcal{D}_0}(\xi)$$

$$\widehat{w}_{a,s}^{(1)}(\xi) = a^{-\frac{1}{4}} \overline{\widehat{\psi}_2(a^{-\frac{1}{2}}(\frac{\xi_1}{\xi_2} - s))} \chi_{\mathcal{D}_1}(\xi),$$

where  $\mathcal{D}_0 = \{(\xi_1, \xi_2) \in \widehat{\mathbb{R}}^2 : |\frac{\xi_2}{\xi_1}| \leq 1\}$ ,  $\mathcal{D}_1 = \{(\xi_1, \xi_2) \in \widehat{\mathbb{R}}^2 : |\frac{\xi_1}{\xi_2}| \leq 1\}$ . For  $a < 1$ ,  $|s| \leq 1$ ,  $t \in \mathbb{R}^2$ ,  $d = 0, 1$ , the Fourier transform of the shearlets can be expressed as

$$\widehat{\psi}_{a,s,t}^{(d)}(\xi) = a V^{(d)}(a\xi) \overline{\widehat{w}_{a,s}^{(d)}(\xi)} e^{-2\pi i \xi t},$$

where  $V^{(0)}(\xi_1, \xi_2) = \widehat{\psi}_1(\xi_1)$ ,  $V^{(1)}(\xi_1, \xi_2) = \widehat{\psi}_1(\xi_2)$ . The continuous shearlet transform of  $u \in L^2(\mathbb{R}^2)$  is:

$$\mathcal{SH}_\psi^{(d)} u(a, s, t) = a \int \widehat{u}(\xi) V^{(d)}(a\xi) \overline{\widehat{w}_{a,s}^{(d)}(\xi)} e^{2\pi i \xi t} d\xi, \quad (\text{III.7})$$

where  $d = 0, 1$  correspond to the horizontal and vertical transforms, respectively. Hence, from (III.7) we have that

$$\mathcal{SH}_\psi^{(d)} u(a, s, t) = v_a^{(d)} u * w_{a,s}^{(d)}(t) \quad (\text{III.8})$$

where

$$v_a^{(d)} u(t) = \int_{\mathbb{R}^2} a \widehat{u}(\xi) V^{(d)}(a\xi) e^{2\pi i \xi t} d\xi.$$

To obtain a transform with the ability to detect edges effectively, we choose the functions  $\widehat{\psi}_1$  to be odd and  $\widehat{\psi}_2$  to be even.

We are now ready to derive an algorithmic procedure to compute a discrete version of (III.8). For  $N \in \mathbb{N}$ , an  $N \times N$  image can be considered as a finite sequence  $\{u[n_1, n_2] : n_1, n_2 = 0, \dots, N-1\}$ . Thus, identifying the domain with  $\mathbb{Z}_N^2$ , we view  $\ell^2(\mathbb{Z}_N^2)$  as the discrete analog of  $L^2(\mathbb{R}^2)$ . Consistently with this notation, the inner product of the images  $u_1$  and  $u_2$  is defined as

$$\langle u_1, u_2 \rangle = \sum_{n_1=0}^{N-1} \sum_{n_2=0}^{N-1} u_1[n_1, n_2] \overline{u_2[n_1, n_2]},$$

and, for  $-N/2 \leq k_1, k_2 < N/2$ , its 2D Discrete Fourier Transform (DFT)  $\widehat{u}[k_1, k_2]$  is given by:

$$\widehat{u}[k_1, k_2] = \frac{1}{N} \sum_{n_1, n_2=0}^{N-1} u[n_1, n_2] e^{-2\pi i (\frac{n_1}{N} k_1 + \frac{n_2}{N} k_2)}.$$

We adopt the convention that brackets  $[\cdot, \cdot]$  denote arrays of indices, and parentheses  $(\cdot, \cdot)$  denote function evaluations. We shall interpret the numbers  $\hat{u}[k_1, k_2]$  as samples  $\hat{u}[k_1, k_2] = \hat{u}(k_1, k_2)$  from the trigonometric polynomial  $\hat{u}(\xi_1, \xi_2) = \sum_{n_1, n_2=0}^{N-1} u[n_1, n_2] e^{-2\pi i(\frac{n_1}{N}\xi_1 + \frac{n_2}{N}\xi_2)}$ .

To implement the directional localization associated with the shearlet decomposition described by the window functions  $w_{a,s}^{(d)}$ , we will compute the DFT on a grid consisting of lines across the origin at various slopes called the *pseudo-polar grid*, and then apply a one-dimensional band-pass filter to the components of the signal with respect to this grid. To do this, let us define the pseudo-polar coordinates  $(\zeta_1, \zeta_2) \in \mathbb{R}^2$  by:

$$\begin{aligned} (\zeta_1, \zeta_2) &= (\xi_1, \frac{\xi_2}{\xi_1}) \quad \text{if } (\xi_1, \xi_2) \in \mathcal{D}_0; \\ (\zeta_1, \zeta_2) &= (\xi_2, \frac{\xi_1}{\xi_2}) \quad \text{if } (\xi_1, \xi_2) \in \mathcal{D}_1. \end{aligned}$$

Using this change of coordinates, we obtain

$$\begin{aligned} \widehat{v}_a^{(d)} f(\zeta_1, \zeta_2) &= \widehat{v}_a^{(d)} f(\xi_1, \xi_2), \\ \widehat{w}^{(d)}(a^{-1/2}(\zeta_2 - s)) &= \widehat{w}_{a,s}^{(d)}(\xi_1, \xi_2). \end{aligned}$$

This expression shows that the different directional components are obtained by simply translating the window function  $\widehat{w}^{(d)}$ . For an illustration of the mapping from the Cartesian grid to the pseudo-polar grid, see Figure 3.

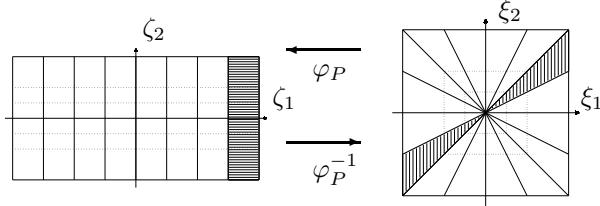


Fig. 3. The mapping  $\varphi_P$  from a Cartesian grid to a pseudo-polar grid. The shaded regions illustrate the mapping  $\varphi_P^{-1}(\hat{\delta}_P[k_1, k_2] \widehat{w}^{(d)}[a^{-1/2}k_2 - \ell])$ , for fixed  $a, \ell$ .

At the scale  $a = 2^{-2j}$ ,  $j \geq 0$ , we will denote by  $v_j^{(d)} u[n_1, n_2]$  the discrete samples of a function  $v_{2^{-2j}}^{(d)} u(x_1, x_2)$ , whose Fourier transform is  $\widehat{v}_a^{(d)} u(\xi_1, \xi_2)$ . Also, the discrete samples  $\widehat{v}_j^{(d)} u[k_1, k_2] = \widehat{v}_{2^{-2j}}^{(d)} u(k_1, k_2)$  are the values of the DFT of  $v_a^{(d)} u[n_1, n_2]$  on the pseudo-polar grid. One may obtain the discrete Frequency values of  $v_a^{(d)} u$  on the pseudo-polar grid by direct extraction using the Fast Fourier Transform (FFT) with complexity  $O(N^2 \log N)$  or by using the Pseudo-polar DFT (PDFFT) with the same complexity.

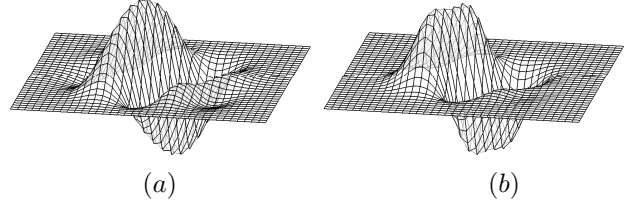


Fig. 4. Examples of spline based shearlets. Figure (a) corresponds to  $\ell = 5$  using a support window of size 16. Figure (b) corresponds to  $\ell = 2$  using a support window of size 8.

To discretize the window function, consider a function  $\widehat{w}^{(d)}$  such that  $\sum_{d=0}^1 \sum_{\ell=-2^j}^{2^j-1} \widehat{w}^{(d)}[2^j k_2 - \ell] = 1$ . That is, the shearing variable  $s$  is discretized as  $s_{j,\ell} = 2^{-j}\ell$ . Letting  $\varphi_P$  be the mapping function from the Cartesian grid to the pseudo-polar grid, the discrete shearlet transform can thus be expressed in the discrete frequency domain as

$$\varphi_P^{-1}(\widehat{v}_j^{(d)} u[k_1, k_2]) \varphi_P^{-1}(\hat{\delta}_P[k_1, k_2] \widehat{w}^{(d)}[2^j k_2 - \ell]),$$

where  $\hat{\delta}_P$  is the discrete Fourier transform of the Dirac delta function  $\delta_P$  in the pseudo-polar grid. Thus, the discrete shearlet transform can be expressed as the discrete convolution

$$\mathcal{SH}^{(d)} u[j, \ell, k] = v_j^{(d)} u * w_{j,\ell}^{(d)}[k],$$

where  $\widehat{w}_{j,\ell}^{(d)}[k_1, k_2] = \varphi_P^{-1}(\hat{\delta}_P[k_1, k_2] \widehat{w}^{(d)}[2^j k_2 - \ell])$ .

The discrete shearlet transform will be computed as follows. Let  $H_j$  and  $G_j$  be the low-pass and high-pass filters of a wavelet transform with  $2^j - 1$  zeros inserted between consecutive coefficients of the filters  $H$  and  $G$ , respectively. Given 1-dimensional filters  $H$  and  $G$ , define  $u * (H, G)$  to be the separable convolution of the rows and the columns of  $u$  with  $H$  and  $G$ , respectively. Notice that  $G$  is the wavelet filter corresponding to  $\psi_1$  where  $\psi_1$  must be an odd function and  $H$  is the filter corresponding to the coarse scale. Finally as indicated above, the filters  $\widehat{w}^{(d)}$  are related to the function  $\psi_2$ , which must be an even function and can be implemented using a Meyer-type filter. Hence, we have:

#### Discrete Shearlet Cascade Algorithm.

Let  $u \in \ell^2(\mathbb{Z}_N^2)$ . Define

$$\begin{aligned} S_0 u &= u \\ S_j u &= S_{j-1} u * (H_j, H_j), \quad j \geq 1. \end{aligned}$$

For  $d = 0, 1$ , the discrete shearlet transform is given by

$$\mathcal{SH}^{(d)} u[j, \ell, k] = v_j^{(d)} u * w_{j,\ell}^{(d)}[k],$$

where  $j \geq 0$ ,  $-2^j \leq \ell \leq 2^j - 1$ ,  $k \in \mathbb{Z}^2$  and  $v_j^{(0)}u = S_j u * (G_j, \delta)$ ,  $v_j^{(1)}u = S_j u * (\delta, G_j)$ .

For simplicity of notation, it will be convenient to combine the vertical and horizontal transforms ( $d = 0, 1$ ) by re-labeling the orientation index  $\ell$  as follows:

$$\mathcal{SH}u[j, \ell, k] = \begin{cases} \mathcal{SH}^{(0)}u[j, \ell - 1 - 2^j, k], & 1 \leq \ell \leq 2^{j+1}; \\ \mathcal{SH}^{(1)}u[j, 3(2^j) - \ell, k], & 2^{j+1} < \ell \leq 2^{j+2}. \end{cases}$$

Using the new notation, at the scale  $a = 2^{-4}$  ( $j = 2$ ), the index  $\ell$  of the discrete shearlet transform  $\mathcal{SH}u[2, \ell, k]$  ranges over  $\ell = 1, \dots, 16$ . Here the first (respectively, last) eight indices correspond to the orientations associated with the horizontal (resp. vertical) transform  $\mathcal{SH}^{(0)}$  (resp.  $\mathcal{SH}^{(1)}$ ).

In our implementation, we use the finite impulse response filters  $H$  and  $G$  that correspond to a quadratic spline wavelet. A reflexive boundary condition on the borders of the image is assumed for the convolution operation. For an  $N \times N$  image, the numerical complexity of the shearlet transform is  $O(N^2 \log(N))$ . In some experiments, non-dyadic scaling will be used, i.e. no zeros will be inserted in the filters  $H_j$  and  $G_j$ .

Figure 4 displays examples of shearlets associated with the discrete shearlet transform. Figure 5 shows the shearlet coefficients  $\mathcal{SH}u[j, \ell, k]$ , where  $u$  is the characteristic function of a disk, at multiple scales, for several values of the orientation index  $\ell$ .

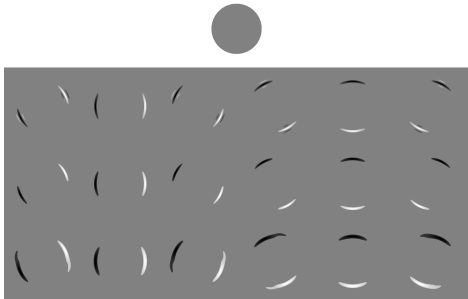


Fig. 5. A representation of shearlet coefficients of the characteristic function of a disk (shown above), at multiple scales (ordered by rows), for several values of the orientation index  $\ell$  (ordered by columns).

The directionally oriented shearing filters have the special feature that  $\sum_{\ell, d} w_{j, \ell}^{(d)} * f = f$ . As a consequence, a unified map of directionally-captured edge elements can be assembled through a simple summation. Other directionally oriented filters such as steerable Gaussian filters do not typically share this property [29, Ch.2].

#### IV. ANALYSIS AND DETECTION OF EDGES

As explained above, a main feature of the shearlet transform is its superior directional selectivity with re-

spect to traditional edge detectors. For example, Figure 2 compares the behavior of the discrete shearlet transform of an image at the edge points with that of the traditional wavelet transform. The figure displays the magnitudes of the discrete shearlet transform  $\mathcal{SH}u[j, \ell, k]$  at the edge points of a star-like image  $u$ , as a function of the scaling index  $j$ , for two different values of the directional variable  $\ell$ . The test shows that the values  $|\mathcal{SH}u[j, \ell, k]|$  are much larger when  $\ell$  corresponds to the normal direction to the edge, in accordance with the theoretical predictions from Section II. Since the wavelet transform has no variable associated with the orientation, its magnitudes do not depend on the orientation.

#### A. Shearlet-based Orientation Estimation

The discrete shearlet transform can be applied to provide a very accurate description of the edge orientations. We will show that this approach has several advantages with respect to traditional edge orientation extraction methods.

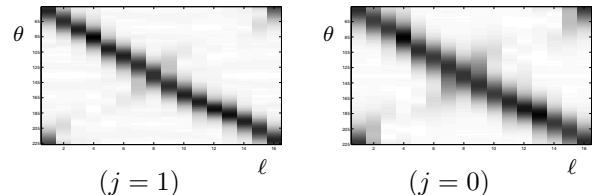


Fig. 6. The directional response of the shearlet transform  $DR(\theta, \ell, j)$  is plotted as a greyscale value, for  $j = 1, 0$ . The orientations  $\theta$  of the half-planes range over the interval  $[45, 225]$  (degrees),  $\ell$  ranges over  $1, \dots, 16$ .

Recall that, in the continuous model where the edges of  $u$  are identified as local maxima of its gradient, the edge orientation is associated with the orientation of the gradient of  $u$ , an idea used, for instance, in the Canny edge detector. Similarly, using the continuous wavelet transform  $W_\psi u(a, t)$ , the orientation of the edges of an image  $u$  can be obtained by looking at the horizontal and vertical components of  $W_\psi u(a, t)$ . In fact, letting  $\psi_a = \nabla G_a$  and  $\psi_a^x = \frac{\partial G_a}{\partial x}$ ,  $\psi_a^y = \frac{\partial G_a}{\partial y}$ , the edge orientation of  $u$  at  $\tau$  is given

$$\arctan \left( \frac{u * \psi_a^y(\tau)}{u * \psi_a^x(\tau)} \right). \quad (\text{IV.9})$$

According to (I.2), the expression (IV.9) measures the direction of the gradient  $\nabla u_a$  at  $\tau$ .

Unfortunately, the gradient model is not very accurate in the presence of noise or when the edge curve is not regular. Furthermore, in the usual numerical implementations, the operator  $\frac{\partial}{\partial x}$  is approximated by a finite difference and this becomes a significant source of inaccuracies in edge orientation estimation.

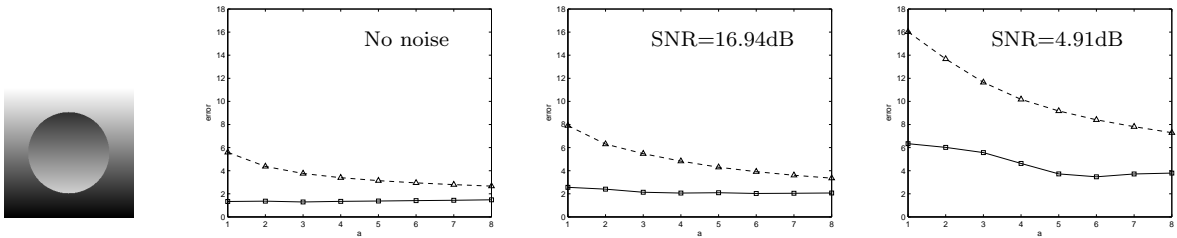


Fig. 7. Comparison of the average error in the estimation of edge orientation (expression (IV.11)), for the disk image shown on the left, using the wavelet method (dashed line) versus the shearlet method (solid line), as a function of the scale  $a$ , for various SNRs (additive white Gaussian noise).

The advantage of the orientation estimation based on the shearlet transform is that, by decomposing an image with respect to scale, location and orientation variables, the orientation information at each scale is directly available. In addition, we can identify not only the ‘dominant’ orientation at a certain point, but a vector of all orientation ‘components’ present at that point. This provides a general orientation representation which will be further exploited in Section IV.B to analyze corner points and junctions.

Other useful ideas to estimate edge orientation have appeared in the literature. For example, the method used by Perona in [30] to estimate edge orientations, which is based on anisotropic diffusion, is very robust in the presence of noise. In contrast to the shearlet approach, however, this method only yields a single orientation estimation and is unable to handle the situation where multiple orientations are present, such in the presence of corner points or junctions. Other researchers view orientation estimation as a local fitting problem [31], [32] which, under least square criterion, is equivalent to PCA analysis. This method is numerically stable and efficient but loses the scaling nature of orientation and, again, only estimates a single orientation (which could be an average of many orientation components at the same point).

As a first experiment, we demonstrate the directional sensitivity of the discrete shearlet transform by measuring its ability to detect edge orientations for a class of test images. Namely, consider the collection of images  $u_\theta$ , representing half-planes at various orientations:

$$u_\theta(x, y) = \chi_{D_\theta}(x, y), \quad D_\theta = \{(x, y) : \frac{y}{x} \leq \tan(\theta)\}.$$

Let  $E$  be the set of edge points of  $u_\theta$  and  $|E|$  be the number of elements in the set  $E$ . We define the *directional response* of shearlet transform at the edge points as the function:

$$DR(\theta, \ell, j) = \frac{1}{|E|} \cdot \sum_{k \in E} |SHu_\theta[j, \ell, k]|$$

Due to its directional sensitivity, at a fixed scale  $2^{-2j}$ , most of the energy of the discrete shearlet transform will be concentrated at a few values of the orientation index  $\ell$ . This is illustrated in Figure 6 for two different values of  $j$  (in both cases, 16 values of the directional index  $\ell$  have been considered).

The above experiment confirms the theoretical properties described in Section II and shows that the discrete shearlet transform is very effective in indicating the orientation of the edges of a digital image. Thus, following Theorem II.1, we propose to estimate the edge orientation of an image  $u$ , at fine scales ( $a = 2^{-2j}$  “small”), by measuring the index  $\tilde{\ell}$  which maximizes the magnitude of the  $SHu[j, \ell, k]$ :

$$\tilde{\ell}(j, k) = \arg \max_{\ell} |SHu[j, \ell, k]|. \quad (IV.10)$$

Once this is found, we can compute  $\theta_S(j, k)$ , the angle of orientation associated with the index  $\tilde{\ell}(j, k)$ .

Notice that, since we are working with a *discrete* transform, this procedure only yields a discrete set of possible orientations since  $\ell$  ranges over a finite set. For example,  $\ell$  ranges over  $1, \dots, 16$  for  $j = 2$ . To improve the accuracy of the orientation estimation and reduce the quantization error, we will interpolate the values of the angle orientation as follows. We will assume that, at an edge point  $t$ , the continuous shearlet transform  $SH_\psi u(a, s, t)$  is essentially a parabolic function with respect of the  $s$  variable, and its maximum occurs for  $s_{\max}$  corresponding to the edge normal orientation. Hence, for  $j$  and  $k$  fixed, we will estimate the angle  $\theta_{\max}$  associated at  $s_{\max}$  using the following algorithm.

#### Shearlet Orientation Detection Algorithm.

- Compute  $\ell_1 = \tilde{\ell}$  using (IV.10); let  $\ell_0 = \ell_1 - 1$ ,  $\ell_2 = \ell_1 + 1$  (here the sums are meant to be modulus  $N$ , where  $N$  is the size of the set of indices  $\ell$ ).
- For  $i = 0, 1, 2$ , let  $\theta_i$  be the angles of orientation associated with the indices  $\ell_i$ .
- Let  $S(\theta) = c_1\theta^2 + c_2\theta + c_3$ , where  $S(\theta_i)$  is identified with  $SHu[j, \ell_i, k]$ ,  $i = 0, 1, 2$ . Then  $c_1, c_2, c_3$  is the

solution of linear system  $S(\theta_i) = c_1\theta_i^2 + c_2\theta_i + c_3$ . So  $\theta_{\max} = -\frac{c_2}{2c_1}$  (this is the value where the parabolic function  $S(\theta)$  achieves its maximum).

Notice that, by construction, the function  $S(\theta)$  is always concave down, and its maximum is close to the orientation associated with  $\tilde{\ell}(j, k)$ .

Extensive numerical experiments demonstrate the ability of this approach to provide a very accurate measure of the edge orientation. An example of application of this algorithm is illustrated in Figure 7, using as a test image a smooth function with an edge along the boundary of a disk. The figure displays the average angular error in the estimate of the edges orientation, as a function of the scale  $a = 2^{-2j}$ , where the *average angle error* is defined by

$$\frac{1}{|E|} \cdot \sum_{t \in E} |\tilde{\theta}(t) - \theta(t)|, \quad (\text{IV.11})$$

$E$  is the set of edge points,  $\theta$  is the exact angle and  $\tilde{\theta}$  the estimated angle. The average angle error using shearlets is compared to that obtained using the wavelet approach, where the edge orientation is estimated using (IV.9). Recall that this approach, for a single scale, is equivalent to the estimation obtained from Canny’s algorithm. Tests reported in Figure 7 show that the shearlet approach significantly outperforms the wavelet method, especially at finer scales, and is extremely robust in the presence of noise. Note the experiments shown in Figure 7 are a base line comparison between the wavelet and shearlet multiscale representations. Additional filtering or additional feature extractions could be used to improve their noise response.

If a pixel  $k$  correspond to a junction or a corner point, then the orientation index  $\tilde{\ell}(j, k)$ , given by (IV.10), will identify the orientation of the ‘strongest’ edge. A more precise analysis of this situation is discussed in the next section.

### B. Feature classification

Consider a simple image  $u$  containing edges and smooth regions, like the one illustrated in Figure 8(a), and examine the behavior of the discrete shearlet transform  $\mathcal{SH}u[j, \ell, k]$ , at a fixed scale  $j_0$ , for some typical locations  $k_0$ . As Figure 8 shows, we can recognize four classes of points from the plot of  $s_{k_0}(\ell) = |\mathcal{SH}u[j_0, \ell, k_0]|$ . Namely, at the junction point  $k_0 = A$ ,  $s_{k_0}(\ell)$  exhibit three peaks corresponding to the orientations of the three edge segments converging into  $A$ ; at the point  $k_0 = B$  on a smooth edge,  $s_{k_0}(\ell)$  has a single peak; at a point  $k = D$  in a smooth region,  $s_{k_0}(\ell)$  is essentially flat; finally, at a point  $k_0 = C$  “close” to an edge,  $s_{k_0}(\ell)$  exhibit two peaks (however they are much

smaller in amplitude than those for the points  $A$  and  $B$ ). The same behavior holds, essentially, for more general images, even in the presence of additive white Gaussian noise (provided, of course, that the SNR is not too small). In particular, at corner points, the behavior is similar to that of point  $A$ , with the plot  $s_A(\ell)$  showing two main peaks corresponding to the orientations of the two segments converging to the corner point.

This suggests to devise a strategy for classifying smooth regions, edges, corners and junctions based on the plot patterns of Figure 8(b). We will proceed in two steps. Let  $j = j_0$  be a fixed (fine) scale. First, since the magnitude of the discrete shearlet transform coefficients at the points along the boundaries (including smooth edges, corners and junctions) is significantly larger than at the other points, they can be easily separated by looking at the energy function at  $k$ :

$$E(k) = \sum_{\ell} |\mathcal{SH}u[j_0, \ell, k]|^2.$$

We will refer to these points with large amplitude values as *boundary points*.

Next, once the boundary points have been separated, we will examine the “form” of the function  $s_k(\ell)$  to distinguish edge points from corners and junction points. That is, a point  $k$  is recognized as a regular edge point if the corresponding function  $s_k(\ell)$  has a single peak. If more than one peak is present,  $k$  will be a corner or a junction point.

Thus, for each boundary point  $k$ , let  $P_k = \{p_k(\ell) : \ell = 1, \dots, N\}$  where  $p_k(\ell)$  is the normalized peak value in the  $\ell$  orientation and is given by

$$p_k(\ell) = \begin{cases} \frac{|\mathcal{SH}u[j_0, \ell, k]|}{\sum_{\ell \in L_k} |\mathcal{SH}u[j_0, \ell, k]|}, & \ell \in L_k; \\ 0, & \ell \notin L_k. \end{cases}$$

and  $L_k$  is the set of orientations where local maxima of the discrete shearlet transform occur, that is,

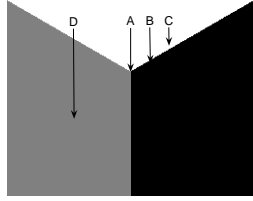
$$L_k = \{\ell : |\mathcal{SH}u[j_0, \ell, k]| > |\mathcal{SH}u[j_0, \ell + 1, k]| \text{ and } |\mathcal{SH}u[j_0, \ell, k]| > |\mathcal{SH}u[j_0, \ell - 1, k]|\}.$$

We present the following algorithm which uses the  $K$ -mean clustering algorithm [33, Ch.10]:

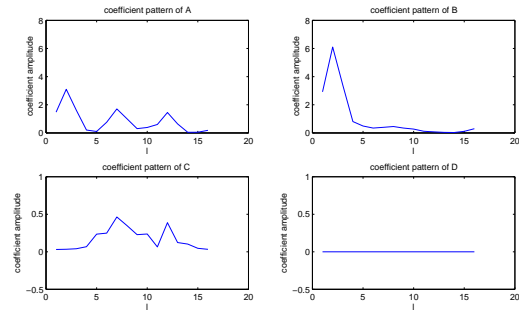
#### Feature Classification Algorithm

- Using the Energy  $E(k)$  as the feature function, we apply the  $K$ -Mean clustering algorithm, with Euclidean metric, to cluster the image points into three sets  $I_1, I_2, I_3$ . Namely, let  $\Omega$  denote the set of points  $I_{i_{max}}$ , where

$$i_{max} = \arg \max_i \frac{1}{|I_i|} \sum_{k \in I_i} E(k).$$



(a)



(b)

Fig. 8. (a) Representative points on the test image. (b) Shearlet Transform pattern  $s(\ell)$ , as a function of  $\ell$  for the points indicated in (a).

$\Omega$  is identified as the set of boundary points. Let  $R$  be the set  $I_{i_{min}}$ , where

$$i_{min} = \arg \min_i \frac{1}{|I_i|} \sum_{k \in I_i} E(k).$$

$R$  is the set of regular points. The remaining set  $I_i$  contains the near edge points.

- For a point  $k$  in  $I_{i_{max}}$ , sort the entries of the vector  $P_k$  as

$$[\tilde{p}_k(1), \dots, \tilde{p}_k(N)],$$

where  $\tilde{p}_k(1) = \max\{p_k(\ell) \in P_k\}$ ,  $\tilde{p}_k(2) = \max\{p_k(\ell) \in P_k \setminus \{\tilde{p}_k(1)\}\}$ , and so on. Then using again the  $K$ -Mean clustering algorithm on  $I_{i_{max}}$ , the set is further classified in two groups corresponding to smooth edge points in one set, corner and junction points in the other set.

It is clear that the algorithm described above can be further refined to distinguish corner points from junction points, and different classes of junction points having different geometric features.

Figure 9 illustrates the application of the Feature Classification Algorithm to three test images, at scale  $j = 0$ , using  $N = 16$  orientations. The results show the separation of the image points into four classes: corners and junctions (Figures b1-b3); smooth edges (Figures c1-c3); near-edge points (Figures d-d3); regular points in smooth regions (Figures e1-e3).

This shows that the shearlet approach provides a very simple and computationally efficient framework for classifying several features of interest in an image. This has some advantages with respect to wavelet-based methods and other existing methods which do not have a specific ability to capture the directional features of an image. For example, using wavelets, in order to identify corner points, one has to design a set of filters which is very different from the one used to detect the smooth edges

[29]. Furthermore, even in this case, the wavelet approach is unable to provide specific information about the geometry of the corners or junctions because it is based on isotropic filters (e.g., the 2D Mexican hat [29]).

### C. Edge Detection Strategies

The shearlet transform provides a multiscale and multi-directional framework which can be used to devise several effective edge detection schemes. In the context of edge detection, it was shown in several studies that one can take advantage of the multiscale decomposition of images to improve the robustness of an edge detector in the presence of noise. In what follows, we will adapt these ideas to propose several multiscale edge detection schemes.

As in the wavelet approach, we will select the edge point candidates of an image  $u$  by first identifying the shearlet transform *modulus maxima*, that is, those points  $(\bar{n}_1, \bar{n}_2)$  which, at fine scales  $j$ , are local maxima of the function

$$M_j u[n_1, n_2]^2 = \sum_{\ell} (\mathcal{SH}u[j, \ell, n_1, n_2])^2.$$

According to the results from Section II, we expect that, if  $(\bar{n}_1, \bar{n}_2)$  is an edge point, the shearlet transform of  $u$  will behave as

$$|\mathcal{SH}u[j, \ell, \bar{n}_1, \bar{n}_2]| \sim C 2^{-\beta j},$$

where  $\beta \geq 0$ .

If, however,  $\beta < 0$  (in which case the size of  $|\mathcal{SH}u|$  increases at finer scales), then  $(\bar{n}_1, \bar{n}_2)$  will be recognized as a delta-type singularity and the point will be classified as noise. Notice that a similar behavior holds for the wavelet transform and it is similarly used for edge detection. The sign of  $\beta$  can be estimated by computing the best linear fit to the data

$$\{\log |\mathcal{SH}u[j, \ell, \bar{n}_1, \bar{n}_2]| \}_{j=1}^J,$$

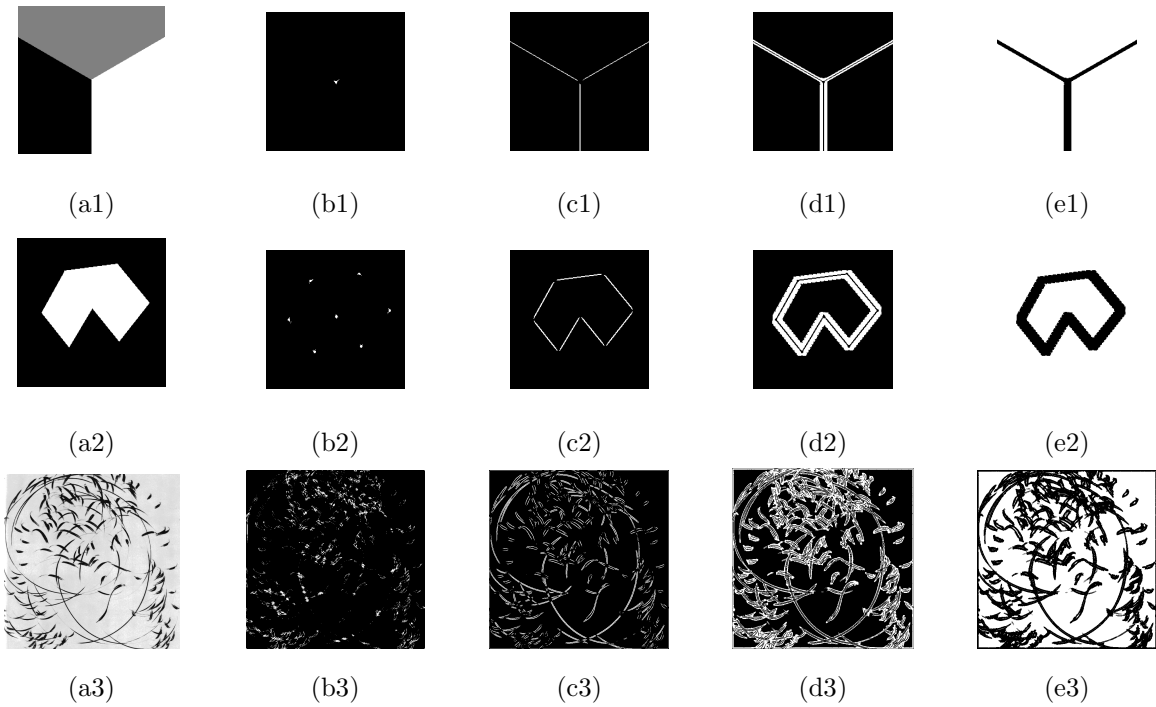


Fig. 9. ((a1-a3) *Test images*. ((b1-b3) *Identification of corners and junctions*. ((c1-c3) *Identification of smooth edge points*. ((d1-d3) *Identification of points near the edges*. ((e1-e3) *Identification of regular points (smooth regions)*).

for the various values of  $\ell$ , where  $J$  is the last decomposition level.

Using this procedure, edge point candidates for each of the oriented components are found by identifying the points for which  $\beta \geq 0$ . These components can then be stitched together by simply adding them up, or using additional constraints. Next, a *non-maximal suppression routine* is applied to these points to trace along the edge in the edge direction and suppress any pixel value that is not considered to be an edge. The non-maximal suppression routine is a standard routine in the Canny edge detector [11]. Using this routine, at each edge point candidate, the magnitude of the shearlet transform is compared with the values of its neighbors along the gradient direction (this is obtained from the orientation map of the shearlet decomposition). If the magnitude is smaller, the point is discarded; if it is the largest, it is kept. This yields a set of possible edge points denoted by  $e_0$ . Finally, the set of edge points can be further refined by

$$\{[n_1, n_2] : e_0[n_1, n_2] \geq T, e_0 * h[n_1, n_2] \geq 0\},$$

where  $h$  is a windowing filter and  $T > 0$  is an appropriate threshold.

Numerical tests have shown that this procedure is very effective at detecting edges. Its computational complexity, however, is too high for practical use. For

this reason we suggest the following modification, which follows essentially the same ideas, and uses the cascade algorithm of the discrete shearlet transform to “reinforce” the true edges and suppress the false ones.

**Shearlet Edge Detection algorithm.** *Given a function  $u \in \ell^2(\mathbb{Z}_N^2)$ , let  $\mathcal{SH}^{(d)}u[j, \ell, k]$  be the discrete shearlet transform, given by*

$$\mathcal{SH}^{(d)}u[j, \ell, k] = v_j^{(d)}u * w_{j, \ell}^{(d)}[k],$$

for  $j \geq 0, -2^j \leq \ell \leq 2^j - 1, k \in \mathbb{Z}^2, d = 0, 1$ , where  $v_j^{(0)}u = S_j u * (G_j, \delta)$ ,  $v_j^{(1)}u = S_j u * (\delta, G_j)$ , and  $S_j u = S_{j-1} u * (H_j, H_j)$ . Set

$$\chi_\ell^{(d)}[k] = \begin{cases} 1 & \text{if } |\mathcal{SH}^{(d)}u[j, \ell, k]| > |\mathcal{SH}^{(d)}u[j-1, \ell, k]|, \\ 0 & \text{otherwise,} \end{cases}$$

and

$$R_j^{(d)}u[k] = \sum_\ell \mathcal{SH}^{(d)}u[j, \ell, k] \chi_\ell^{(d)}[k].$$

Then  $v_j^{(d)}u$  is modified as

$$v_j^{(d)}u = \begin{cases} v_j^{(d)}u + R_j^{(d)}u & \text{if } |v_j^{(d)}u| \leq |R_j^{(d)}u| \\ R_j^{(d)}u & \text{otherwise.} \end{cases}$$

The edge candidates  $e_j u$  at level  $j$  are then given by

$$e_j^2 u[k] = \left( \sum_\ell \mathcal{SH}^1 u[j, \ell, k] \right)^2 + \left( \sum_\ell \mathcal{SH}^2 u[j, \ell, k] \right)^2.$$

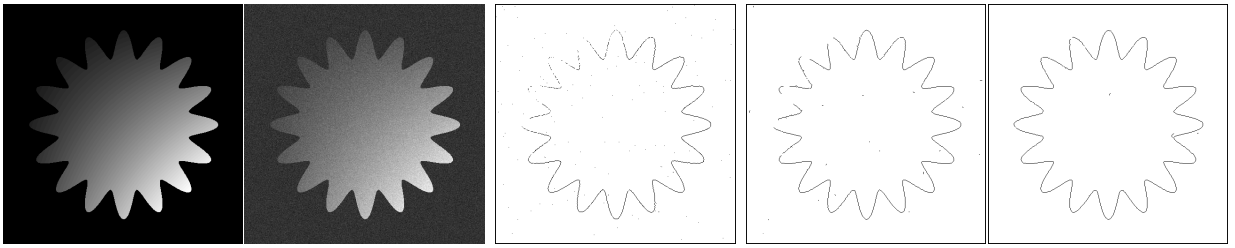


Fig. 10. Results of edge detection methods. From left to right: Original image, noisy image (PSNR=24.61 dB), Sobel result (FOM=0.79), wavelet result (FOM=0.88), shearlet result (FOM=0.92).

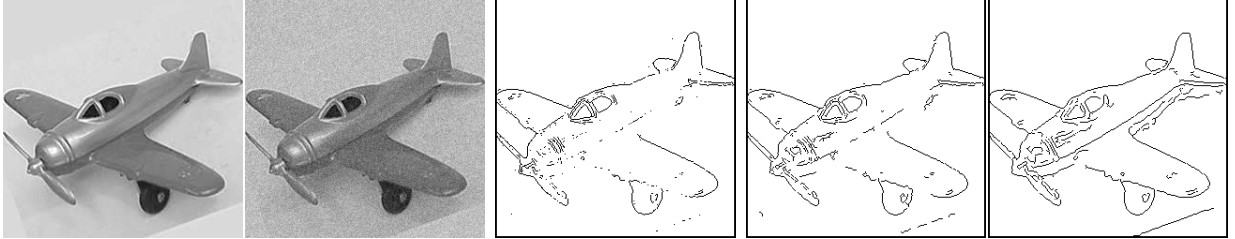


Fig. 11. Results of edge detection methods. From left to right: Original image, noisy image (PSNR=24.58 dB), Sobel result (FOM=0.54), wavelet result (FOM=0.84), and shearlet result (FOM=0.94)



Fig. 12. Results of edge detection methods. From left to right: Original image, noisy image (PSNR=24.61 dB), Sobel result (FOM=0.32), wavelet result (FOM=0.60), and shearlet result (FOM=0.89)

Note that  $v_j^{(d)}u$  is modified to keep the scales small for locations with positive Lipschitz regularity and increase the scales for locations with negative Lipschitz regularity.

The edge candidates for the  $J$ -th level are finally filtered through the application of a non-maximal suppression routine using the shearlet-based orientation map followed by the application of *hysteresis thresholding*. The hysteresis thresholding, which was also included in the original Canny edge detector [11] (see also [34, Ch.7]) is used as a means of eliminating *streaking*. Streaking is the breaking up of an edge contour caused by the edge detector operator output fluctuating above and below a fixed threshold. Indeed, if a single threshold  $T_1$  is applied to an image, then, due to noise, there will be instances where the edge dips below the thresh-

old. To avoid this, hysteresis uses 2 thresholds, a high  $T_1$  and a low  $T_2$ . Any pixel in the image that has a value greater than  $T_1$  is presumed to be an edge pixel, and is marked as such immediately. Then, any pixels that are connected to this edge pixel and that have a value greater than  $T_2$  are also selected as edge pixels.

We have tested several images using the Shearlet Edge Detection algorithm described above, and compared its performance to other well established edge detectors. For the tests reported in Figures 10-12, each of the images had an additive white Gaussian noise with a standard deviation of 20. The shearlet decomposition tested consisted of 4 decomposition levels using 16 directional components. We compared the shearlet-based routine against a similar wavelet-based routine that was derived by removing the shearlet aspect of the algorithm given above. Throughout all experiments the

wavelet and shearlet routines had the same fixed parameters. The comparison against this particular wavelet routine highlights how the anisotropic aspect of shearlets can improve performance in detection. For a baseline comparison against standard routines, we also used the Sobel method using its default parameters [34]. The standard Canny method was not used for comparisons because we found that the default parameters provided very poor results. By adjusting the variance used in the default parameter for each test, better results can be achieved. The issue of how to choose an appropriate variance is exactly why multiscale methods, such as the wavelet-based routine tested, have been suggested.

Several attempts have been made in the literature to propose an objective measure for the performance of an edge detector. While there is no consensus and each of these measures has their limitations, one of the most recognized measure is the *Pratt's Figure of Merit (FOM)* [35], whose definition is based on the combination of three factors: non detection of true edges, detection of false edges and edge delocalization error, which is defined as

$$F = \frac{1}{\max(N_e, N_d)} \sum_{k=1}^{N_d} \frac{1}{1 + \alpha d(k)^2},$$

where  $N_e$  is the number of actual edge points,  $N_d$  is the number of detected edge points,  $d(k)$  is the distance from the  $k$ -th actual edge point to the detected edge point and  $\alpha$  is a scaling constant typically set to  $1/9$ . Hence, the output from Pratt's Figure of Merit is a fidelity function ranging from 0 to 1, where 1 is a perfect edge detector. We computed the Pratt' Figure of Merit using the image shown in Figure 10 based on the actual edge map that is known analytically. The results reported in the following table confirm the visual impression that the shearlet approach outperforms the other edge detectors considered in our tests. The Pratt' Figure of Merit was also computed for the images in Figures 11-12 and the results are reported in the captions of those figures. Since in these cases the exact edge maps were not known, they were computed using the Canny algorithm on the image without noise. The shearlet approach is shown to yield higher values for the Figure of Merit.

| <b>Pratt's FOM for the image of Figure 10</b> |          |         |       |         |
|---|----------|---------|-------|---------|
| PSNR  | Shearlet | Wavelet | Sobel | Prewitt |
| 34.16 dB                                      | 0.94     | 0.93    | 0.88  | 0.87    |
| 28.14 dB                                      | 0.94     | 0.91    | 0.84  | 0.84    |
| 24.61 dB                                      | 0.92     | 0.88    | 0.79  | 0.78    |
| 22.10 dB                                      | 0.76     | 0.67    | 0.67  | 0.69    |

## V. CONCLUSION AND FUTURE DIRECTION

Several concepts based on the shearlet framework presented in this work have a great potential for devising alternative improved edge analysis and detection schemes. Since the notion of analyzing edges by looking at the maxima of the wavelet transform has appeared, a multitude of edge detection algorithms based on this concept have been developed. In this work we have only explored a few of these techniques by using the shearlet transform. Several concepts, such as those in [36], [15], could be further explored and adapted for their use with the shearlet transform. This study shows that the shearlet transform provides a multiscale directional framework which is very competitive for the purpose of edge analysis and detection. This approach is based on a simple and rigorous mathematical theory which accounts for the geometrical properties of edges. In particular, it provides an accurate method for extracting the information about edges and their orientations even in presence of noise. This opens the door to a number of further applications including feature extraction and shape recognition.

## VI. ACKNOWLEDGMENT

The authors would like to thank the referees for their useful comments and suggestions which significantly improved this paper.

## REFERENCES

- [1] S. Mallat and W. L. Hwang, Singularity detection and processing with wavelets, *IEEE Trans. Inf. Theory*, vol. 38, no. 2, 617-643, Mar. 1992.
- [2] S. Mallat and S. Zhong, Characterization of signals from multiscale edges, *IEEE Trans. Pattern Anal. Mach. Intell.*, Vol. 14, no. 7, pp. 710-732, Jul. 1992.
- [3] C. L. Tu, W. L. Hwang, and J. Ho, "Analysis of Singularities From Modulus Complex Wavelets", *IEEE Transactions Inf. Theory*, Vol. 51, n. 3, pp. 1049-1062, 2005.
- [4] L. Zhang, P. Bao, "A Wavelet-based Edge Detection Method by Scale Multiplication", *Pattern Recognition, Proceedings. 16th International Conference on*, Vol. 3, pp. 501-504, Aug. 2002.
- [5] J. Li, A Wavelet Approach to Edge Detection, Masters Thesis, Sam Houston State University, 2003.
- [6] M. N. Do, and M. Vetterli, "The contourlet transform: an efficient directional multiresolution image representation", *IEEE Trans. Image Process.*, vol. 14, no. 12, pp. 2091-2106, Dec. 2005.
- [7] D. D. Po and M. N. Do, "Directional multiscale modeling of images using the contourlet transform", *IEEE Trans. Image Process.*, vol. 15, no. 6, pp. 1610-1620, June 2006.
- [8] I.W.Selesnick, R.G. Baraniuk, and N.G.Kingsbury, "The Dual-Tree Complex Wavelet Transform", *IEEE Signal Processing Magazine* vol. 22(6), 123-151, Nov. 2005.
- [9] E. J. Candès and D. L. Donoho, "Ridgelets: a key to higher-dimensional intermittency?", *Phil. Trans. Royal Soc. London A*, Vol. 357, pp. 2495-2509, 1999.
- [10] E. J. Candès and D. L. Donoho, "New tight frames of curvelets and optimal representations of objects with  $C^2$  singularities", *Comm. Pure Appl. Math.*, Vol. 56, pp. 219-266, 2004.

- [11] F. J. Canny, A computational approach to edge detection, *IEEE Trans. Pattern Anal. Machine Intell.*, Vol. 8, no. 6, 679-698, 1986.
- [12] T. Lindeberg, "Edge detection and ridge detection with automatic scale selection", *Proceedings of the IEEE Int. Conference on Computer Vision and Pattern Recognition*, San Francisco, June 1996, pp. 465-470, 1996
- [13] T. Lindeberg, "Feature Detection with Automatic Scale Selection", *International Journal of Computer Vision*, vol. 30(2), pp. 79-116, 1998.
- [14] S. Mallat, *A Wavelet Tour of Signal Processing*, Academic Press, San Diego, CA, 1998.
- [15] D. Ziou, and S. Tabbone, "Edge Detection Techniques An Overview", *International Journal of Pattern Recognition and Image Analysis*, Vol. 8(4) pp. 537-559, 1998.
- [16] P. Perona, "Steerable-scalable kernels for edge detection and junction analysis", *Image Vis. Comput.*, Vol. 10, pp. 663-672, 1992.
- [17] J. Weickert, Foundations and applications of nonlinear anisotropic diffusion filtering, *Zeitschr. Angewandte Math. Mech.*, Vol. 76, pp. 283-286, 1996.
- [18] J. Geusebroek, A. W. M. Smeulders, and J. van de Weijer, "Fast Anisotropic Gauss Filtering", *IEEE Trans. Image Process.*, Vol. 8, pp. 938-943, 2003.
- [19] G. Easley, D. Labate, and W-Q. Lim "Sparse Directional Image Representations using the Discrete Shearlet Transform", to appear in *Appl. Comput. Harmon. Anal.* 2008.
- [20] D. Labate, W.-Q. Lim, G. Kutyniok and G. Weiss, "Sparse multidimensional representation using shearlets", *Wavelets XI* (San Diego, CA, 2005), SPIE Proc., 5914, pp. 254-262, SPIE, Bellingham, WA, 2005.
- [21] K. Guo and D. Labate, "Optimally sparse multidimensional representation using shearlets", *SIAM J. Math. Anal.*, Vol. 9, pp. 298-318, 2007.
- [22] E. J. Candès and D. L. Donoho, "Continuous curvelet transform: I. Resolution of the wavefront set", *Appl. Comput. Harmon. Anal.*, Vol. 19, pp. 162-197, 2005. 162-197.
- [23] S. Dekel and A. Sherman, "Curvelets: A low-level system for computer vision", preprint 2008.
- [24] W. Freeman and E. Adelson, "The design and use of steerable filters", *IEEE Trans. Patt. Anal. and Machine Intell.*, Vol. 13, pp. 891-906, 1991.
- [25] E. Simoncelli and W. Freeman, "The steerable pyramid: A flexible architecture for multi-scale derivative computation", in *Proc. IEEE ICIP*, Washington, DC, 1995.
- [26] M. Holschneider, *Wavelets. Analysis tool*, Oxford University Press, Oxford, 1995.
- [27] G. Kutyniok and D. Labate, "Resolution of the Wavefront Set using Continuous Shearlets", to appear in *Trans. Am. Math. Soc.*, 2008.
- [28] K. Guo, D. Labate and W. Lim, "Edge analysis and identification using the continuous shearlet transform", to appear in *Appl. Comput. Harmon. Anal.* .
- [29] J. P. Antoine, R. Murenzi, P. Vandergheynst, S. T. Ali, *Two-Dimensional Wavelets and their Relatives*, Cambridge University Press, 2004.
- [30] P. Perona, "Orientation Diffusion", *IEEE Transactions on Image Processing*, Vol.7(3), pp. 457-467, 1998.
- [31] R. Mester, "Orientation Estimation: Conventional Techniques and A New Non-differential Approach", *Proc. 10th European Signal Processing Conf*, 2000.
- [32] J. Bigun, G.H.Granlund, J.Wiklund, "Multidimensional Orientation Estimation with Applications to Texture Analysis and Optical Flow", *IEEE Transactions on Pattern Analysis and Machine Intelligence*, Vol. 13(8), pp. 775-790, 1991.
- [33] R. O. Duda, P. E. Hart, D. G. Stork, *Pattern Classification*, Wiley-Interscience, 2000.
- [34] E. Davies, *Machine Vision: Theory, Algorithms and Practicalities*, Academic Press, 1990.
- [35] W.K. Pratt, *Digital Image Processing*, Wiley Interscience Publications, 1978.
- [36] T. Aydin, Y. Yemes, E. Anarim, B. Sankur, "Multidirectional and Multiscale Edge Detection via *M*-Band Wavelet Transform", *IEEE Trans. Image Process.*, Vol. 5, pp. 1370-1377, 1996.



**Sheng Yi Sheng Yi** received the B.E in electronic and information engineering from Huazhong University of Science and Technology, China, in 2006, and currently in Ph.D. program of electrical engineering department in North Carolina State University. His research interesting includes image representation, shape analysis and high dimensional signal processing.



**Demetrio Labate** Demetrio Labate received the Ph.D. in electrical engineering from the Politecnico di Torino, Italy, in 1995, and the Ph.D. degree in Mathematics from the Georgia Institute of Technology, Atlanta, in 2000. Between 2000 and 2003, he was a Chauvenet lecturer at Washington University in St.Louis. Since 2003, he is an Assistant Professor at North Carolina State University. His research interests include harmonic analysis, with special emphasis on wavelet theory, time-frequency analysis and image processing applications. Prof. Labate received the National Science Foundation CAREER Award in 2008.



**Glenn R. Easley** Glenn R. Easley received the B.S. degree (with honors) and the M.A. degree in mathematics from the University of Maryland, College Park, in 1993 and 1996, respectively, and the Ph.D. degree in computational science and informatics from George Mason University in 2000. Since 2000, he has been working for System Planning Corporation in signal and image processing. He has also been a Visiting Assistant Professor for the Norbert Wiener Center in the University of Maryland since 2005. His research interests include computational harmonic analysis, with special emphasis on wavelet theory and time-frequency analysis, synthetic aperture radar, deconvolution and computer vision.



**Hamid Krim** Hamid Krim received his degrees in Electrical Engineering. As a member of technical staff at AT&T Bell Labs, he has worked in the area of telephony and digital communication systems/subsystems. In 1991 he became a NSF Post-doctoral scholar at Foreign Centers of Excellence (LSS Supelec Univ. of Orsay, Paris, France). He subsequently joined the Laboratory for Information and Decision Systems, MIT, Cambridge, MA, as a Research Scientist performing and supervising research in his area of interest, and later as a faculty in the ECE dept. at North Carolina State University in 1998. He is an original contributor and now an affiliate of the Center for Imaging Science sponsored by the Army. He also is a recipient of the NSF Career Young Investigator award. He is a Fellow of IEEE and was on the editorial board of the *IEEE Trans. on SP* and regularly contributes to the society in a variety of ways. He is a member of SIAM and of Sigma Xi. His research interests are in statistical Signal Processing and mathematical modeling with a keen emphasis on applications.